

Charge-density studies of energetic materials: CL-20 and FOX-7. Corrigendum

A. Meents,^{a*} B. Dittrich,^{b*} S. K. J. Johnas,^a V. Thome^c and E. F. Weckert^a

^aHASYLAB at DESY, Notkestrasse 85, D-22607 Hamburg, Germany, ^bChemistry M313, School of Biomedical, Biomolecular and Chemical Sciences, University of Western Australia, Crawley, WA 6009, Australia, and ^cFraunhofer ICT, Joseph v. Fraunhofer Strasse 7, D-76327 Pfinztal Berghausen, Germany

Correspondence e-mail: alke.meents@desy.de, bdittri@gwdg.de

A corrigendum to the paper by Meents *et al.* (2008), *Acta Cryst. B* **64**, 42–49 to correct the nomenclature for CL-20.

The chemical name for CL-20 was given incorrectly in Meents *et al.* (2008). The correct name is 2,4,6,8,10,12-hexanitro-2,4,6,8,10,12-hexaazaisowurtzitane (common name) or 2,4,6,8,10,12-hexanitro-2,4,6,8,10,12-hexaazatetracyclo[5.5.0.0^{5,9}.0^{3,11}]dodecane (systematic name).

References

Meents, A., Dittrich, B., Johnas, S. K. J., Thome, V. & Weckert, E. F. (2008). *Acta Cryst. B* **64**, 42–49.

Charge-density studies of energetic materials: CL-20 and FOX-7

A. Meents,^{a*} B. Dittrich,^{b*} S. K. J. Johnas,^a V. Thome^c and E. F. Weckert^a

^aHASYLAB at DESY, Notkestrasse 85, D-22607 Hamburg, Germany, ^bChemistry M313, School of Biomedical, Biomolecular and Chemical Sciences, University of Western Australia, Crawley, WA 6009, Australia, and ^cFraunhofer ICT, Joseph v. Fraunhofer Strasse 7, D-76327 Pfingstal Berghausen, Germany

Correspondence e-mail: alke.meents@desy.de, bdittri@gwdg.de

Received 19 May 2007
Accepted 1 November 2007

Experimental electron densities and derived properties have been determined for the two energetic materials CL-20 (3,5,9,11-tetraacetyl-14-oxo-1,3,5,7,9,11-hexaazapentacyclo-[5.5.3.0₂.6.0₄.10.0₈.12]pentadecane), and FOX-7 (1,1-diamino-2,2-dinitroethylene) from single-crystal diffraction. Synchrotron data extending to high scattering angles were measured at low temperature. Low figures-of-merit and excellent residuals were obtained. The Hansen & Coppens multipole-model electron density was compared with results from theoretical calculations *via* structure factors simulating an experiment. Chemical bonding in the molecules is discussed and a topological analysis gives insight especially into the character of those bonds that are thought to play a key role in the decomposition of the molecules. A comparison of theoretical and experimental electrostatic potentials shows no obvious evidence supporting earlier findings on other nitroheterocyclic molecules that electron-density maxima near the C–NO₂ bonds mapped on the electron-density isosurface can be correlated with impact sensitivities. For FOX-7 periodic Hartree–Fock calculations were performed to investigate the influence of the crystal field on the electron density distribution.

1. Introduction

Murray *et al.* (1995) have compiled a list of impact sensitivities for a number of nitroaromatics and nitroheterocycles, and found that these can be related quantitatively to the degrees of internal charge separation and the presence of strongly positive electrostatic-potential (ESP) maxima on their molecular surfaces based on theoretical calculations of isolated molecules. More recently Rice & Hare (2002) have reviewed theoretical efforts. They have extended and modified earlier ideas and procedures and conclude that ‘the level of sensitivity to impact is related to the degree of positive charge build-up over covalent bonds within the inner framework of these explosives’.

In a series of charge-density studies on propellants and explosives, *e.g.* 5-nitro-2,4-dihydro-3H-1,2,4-triazol-3-one (NTO; Zhurova & Pinkerton, 2001), two biguanidinium dinitramides (Zhurova *et al.*, 2004), pentaerythritol tetranitrate (Zhurova *et al.*, 2006) and 1,3,4-trinitro-7,8-diazapentalene (Chen *et al.*, 2007), Pinkerton and coworkers have studied the chemical bonding in these molecules using high-resolution experimental diffraction data. In these studies they have shown that additional insight from the experimental electron-density distribution can be gained when it is compared with theoretical calculations.

High-level theoretical calculations with extended basis sets are currently, except for small molecules and unit cells, limited

Table 1

Data-collection parameters for CL-20 and FOX-7.

For CL-20 the primary beam intensity attenuated to 20%.

Crystal	Run	$\Delta\Phi$	Exposure time (s)	Detector distance (mm)	No. of frames
CL-20	1	0.2	20	33	2989
	2	0.5	120	33	411
	3	1	20	43	1440
	4	0.5	20	43	720
	5	2	10	63	360
	6	2	10	63	360
FOX-7	1	0.5	120	33	1851
	2	1	20	43	710
	3	2	20	63	360
	4	2	10	53	218

to isolated molecules, neglecting the effects of intermolecular interactions and molecular packing on the electron-density distribution. In contrast to isolated molecules, the charge-density distribution from a diffraction experiment represents a molecule as part of the crystal and therefore includes both these effects. Hence, information beyond an isolated-molecule calculation is contained in the experimental data. The main focus of this study is to try to investigate whether or not theoretical findings can be supported by an experimental charge-density study.

In this work we investigate two energetic materials, CL-20 and FOX-7 (Fig. 1). A single-crystal structure determination based on the conventional single-crystal diffraction data of CL-20 (3,5,9,11-tetraacetyl-14-oxo-1,3,5,7,9,11-hexaazapentacyclo-[5.5.3.0.2,6.0.4,10.0.8,12]pentadecane), also called HNIW, was first carried out by Nielsen *et al.* (1998). Other crystallographic works relevant to structural aspects of CL-20 were summarized in a multi-temperature study by Bolotina *et al.* (2004), who examined the temperature-dependent changes in the unit cells (*i.e.* thermal expansion) of the γ and ϵ polymorphs of CL-20. As for FOX-7 Sorescu and co-workers have performed extensive theoretical calculations on CL-20 (Sorescu *et al.*, 1998). CL-20 is very sensitive and accidental initiation is common. Understanding and improving its characteristics in terms of impact sensitivity is of special interest. The structure of FOX-7 (1,1-diamino-2,2-dinitroethylene) has been reported by Bemm & Östmark (1998) and also by Gilardi (1999). In the earlier structure report a comparison of the geometry from a quantum chemical calculation had already been made and good agreement was found. Furthermore, comprehensive high-level quantum mechanical and molecular-mechanics calculations using an isolated molecule, a plain-wave calculation in the solid-state and force-field simulations have been performed (Sorescu *et al.*, 2001) for FOX-7, predicting IR frequencies, estimating the lattice energy and simulating temperature-dependent structural changes. FOX-7 is very insensitive to shock, vibration, fire or impact and its explosive properties are extremely favorable. Owing to high production costs it is not in commercial use to date.

Both molecules are polymorphic. Temperature-dependent phase transitions have been characterized (Kempa & Herr-

mann, 2005) by powder diffraction for FOX-7 for three different polymorphs; Russell *et al.* (1993) have distinguished five polymorphs and provided a pressure/temperature phase diagram for CL-20.

We investigate here the experimental electron density of the ϵ polymorph of CL-20 and of the α polymorph of FOX-7 based on high-resolution X-ray single-crystal diffraction experiments at low temperature using synchrotron radiation. Data were evaluated with a multipole refinement using the Hansen and Coppens model (Hansen & Coppens, 1978), which is based on earlier work of Stewart (1976). Although in principle the electron density can be compared directly between theory and experiment, the quantum mechanical and multipole-model electron-density descriptions generally differ. In order to compare derived topological properties (Bader, 1990), the ESP and the dipole moment using the same density description, we have 'simulated' an X-ray diffraction experiment and calculated structure factors for the isolated molecules based on the quantum chemical single-point electron density using the experimental geometry. The procedure used is explained in §3.1. We have then evaluated these with the same multipole model that is used in the refinement of the experimental data. Experimental bond-topological properties of both molecules are also compared. For FOX-7 the full charge-density analysis includes calculated hydrogen ADPs derived from the TLS + ONIOM method (Whitten & Spackman, 2006). Based on the experimental geometry the interaction density (Spackman *et al.*, 1999) was calculated.

2. Experimental

2.1. Crystal growth

CL-20 was purchased from SNPE (France). The ground material was recrystallized by storing it for 7 d at 333 K in 2-propanol. Using this protocol, nicely shaped crystals of up to 400 microns in size and without any visible growth defects were obtained. In the current version the size description applies to the growth defects rather than to the crystal. FOX-7 powder, purchased from FOI (Sweden), was stored for 7 d at 353 K in acetone. Again, this procedure yielded crystals of up to 500 microns with a well defined morphology and without any visible growth defects.

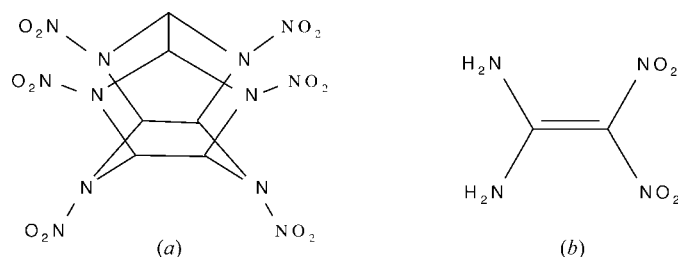


Figure 1
Chemical structures of (a) CL-20 and (b) FOX-7.

Table 2
Experimental details.

	FOX-7	CL-20
Crystal data		
Chemical formula	C ₂ H ₄ N ₄ O ₄	C ₆ H ₆ N ₁₂ O ₁₂
<i>M_r</i>	148.09	438.23
Cell setting, space group	Monoclinic, <i>P</i> 2 ₁ / <i>n</i>	Monoclinic, <i>P</i> 2 ₁ / <i>n</i>
Temperature (K)	100	100
<i>a</i> , <i>b</i> , <i>c</i> (Å)	6.922 (1), 6.501 (1), 11.262 (1)	8.789 (1), 12.474 (1), 13.279 (1)
β (°)	90.485 (1)	106.578 (1)
<i>V</i> (Å ³)	505.8 (1)	1395.31 (2)
<i>Z</i>	4	4
<i>D_x</i> (g cm ⁻³)	1.941 (1)	2.086
Radiation type	Synchrotron radiation, λ = 0.503 Å	Synchrotron radiation, λ = 0.503 Å
μ (mm ⁻¹)	0.185	0.20
Crystal form, color	Prismatic, yellow	Rectangular, colorless
Crystal size (mm)	0.22 × 0.25 × 0.27	0.24 × 0.26 × 0.31
Data collection		
Diffraction method	Beamline E2; HASYLAB-DESY	Beamline E2; HASYLAB-DESY
Data collection method	Rotation photographs	Rotation photographs
Absorption correction	None	None
No. of measured, independent and observed reflections	143 738, 6093, 5329	486 590, 16 427, 14 455
Criterion for observed reflections	<i>I</i> > 3σ(<i>I</i>)	<i>I</i> > 3σ(<i>I</i>)
<i>R</i> _{int}	2.7	2.9
θ _{max} (°)	33.6	33.6
Refinement		
Refinement on	<i>F</i>	<i>F</i>
<i>R</i> [<i>F</i> ² > 2σ(<i>F</i> ²)], <i>wR</i> (<i>F</i> ²), <i>S</i>	0.021, 0.027, 2.05	0.028, 0.033, 1.98
No. of reflections	5329	14 455
No. of parameters	184	360
H-atom treatment	Refined independently	Refined independently
Weighting scheme	<i>w</i> = 1/[σ ² (<i>F_o</i>)]	<i>w</i> = 1/[σ ² (<i>F_o</i>)]
(Δ/σ) _{max}	< 0.0001	< 0.0001
Δρ _{max} , Δρ _{min} (e Å ⁻³)	0.292, -0.359	0.819, -0.512

2.2. Data collection

X-ray single-crystal diffraction experiments were carried out at the HASYLAB (DESY, Hamburg) E2 beamline using a MAR research 'desktop beamline' equipped with a MAR CCD detector. Data collection was performed at 100 K at an X-ray energy of 24.5 keV, corresponding to a wavelength of 0.503 Å. To obtain datasets providing a dynamic range sufficient for a subsequent charge-density analysis several datasets with different exposure times and rotation increments at different detector distances were collected from each crystal. A summary of the data collection parameters is given in Table 1. Data were processed with the *XDS* program package (Kabsch, 1993). In both cases data quality is very high owing to massive redundancy of the data. An overall coverage of more than 99% up to a resolution of approximately 1.1 Å⁻¹ in sin θ/λ (*d* = 0.45 Å) was obtained for both datasets. No significant intensity decay was observed. Further details of crystal data and measurement conditions are given in Table 2.¹

Presently available CCD detectors are optimized for photon energies up to 12 keV, where photons are almost

totally stopped by the fluorescence phosphor independent of the incident angle. For higher photon energies the absorption becomes incomplete and a smaller portion of the diffracted photons is absorbed within the phosphor leading to systematic errors of the measured intensities. This is due to the different path lengths of the photons in the phosphor as diagnosed earlier (Zaleski *et al.*, 1998). In order to take this effect into account, a new correction procedure was applied (Johnas *et al.*, 2006). The correction is based on a comparison of the reflection intensity data of a standard material measured with the area detector used in the experiments and a point detector. The intensities determined with the point detector are, owing to the measurement geometry, not affected by an oblique incidence and were therefore used as a reference dataset. In order to correct the CL-20 and FOX-7 CCD data for the oblique incidence contribution, a corundum dataset with the same experimental parameters as used for the FOX-7 and CL-20 data collections was recorded with the same CCD detector and a point detector. The ratio of reflection intensities depending on the angle of

incidence on the CCD detector surface was approximated by a second-degree polynomial function for both datasets. This fit function was subsequently applied to the CL-20 and FOX-7 intensity data. The detailed procedure and further details will be published in a forthcoming paper.

The molecular structures, thermal movement at 100 K and the atomic-numbering scheme of the title compounds is shown in Fig. 2. In both cases the atomic numbering follows the literature, using the variable-temperature study of Bolotina *et al.* (2004) for CL-20 and the original structure publication (Bemm & Östmark, 1998) for FOX-7.

3. Electron density and ADP modelling

Experimental datasets were modeled by a pseudoatom scattering model (Stewart, 1976) and the Hansen and Coppens multipole formalism (Hansen & Coppens, 1978), as implemented in the program package *XD* (Koritsánszky *et al.*, 2003), was used. The formalism allows a pseudoatom representation of deformations of the electron density ρ(**r**) owing to chemical bonding, including the crystal field (Spackman *et al.*, 1999), and is described in detail in a monograph by Coppens (1997). In the Hansen & Coppens multipole formalism the sum of a

¹ Supplementary data for this paper are available from the IUCr electronic archives (Reference: BS5048). Services for accessing these data are described at the back of the journal.

spherical core, a spherical valence and an aspherical valence density [see (1)] give the total electron density

$$\rho_{\text{atom}}(\mathbf{r}) = \rho_{\text{core}}(r) + P_{\text{val}}\kappa^3\rho_{\text{val}}(\kappa r) + \sum_{l=0}^{l_{\text{max}}} \kappa'^3 R_l(\kappa' r) \sum_{m=0}^l P_{lm\pm} d_{lm\pm}(\theta, \varphi), \quad (1)$$

where l is the order of the multipole expansion, P_{val} , P_{lm} , κ and κ' are refinable multipole parameters, R_l are Slater-type radial functions and d_{lm} are orientation-dependent spherical harmonic functions.

3.1. Multipole models

Chemical constraints were used extensively in both multipole models as the molecules consist of the same functional groups with identical local chemical environments. For CL-20 multipole populations of O2-12 were constrained to O1, those of N3,5,7,9,11 to N1, those of N4,6,8,10,12 to N2, those of C3,5,7,9 to C1 and those of H2-6 to H1. The local atomic site

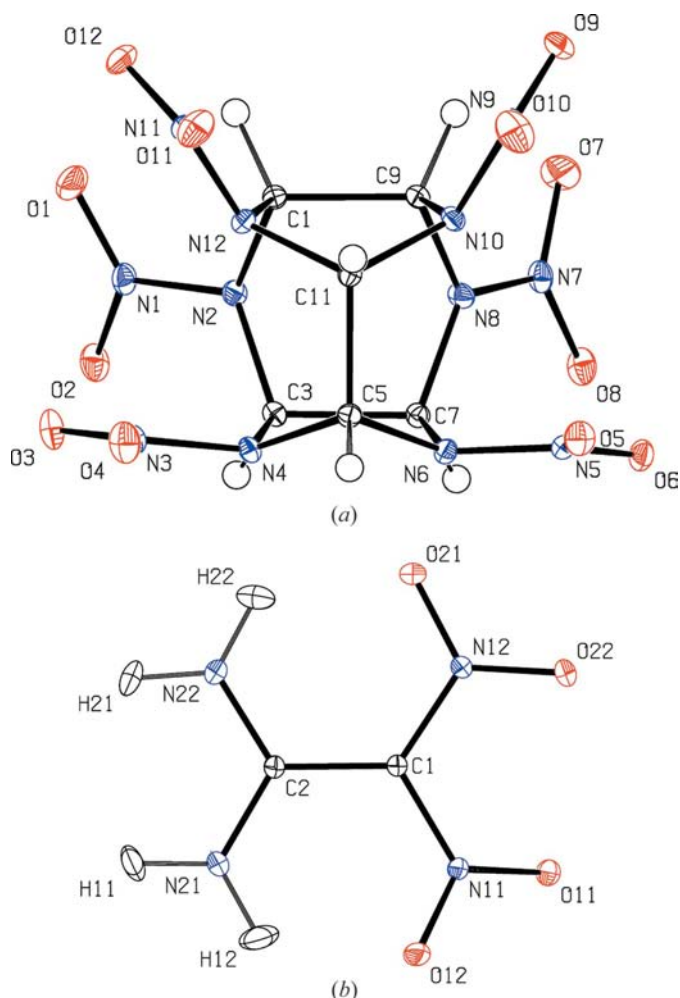


Figure 2
ORTEP representation (Burnett & Johnson, 1996) of (a) CL-20 and (b) FOX-7 illustrating molecular structure and thermal motion in the two crystals at 100 K and including atomic numbering schemes. Hydrogen ADPs for FOX-7 were calculated. Displacement ellipsoids are at 50% probability.

symmetry used was 1 for oxygen, m for N1,2 and 2 for C1. Whereas the chemically equivalent sets of N, C and H atoms share a very similar environment and differ only in their intermolecular interaction, and to a very small degree in their conformation, O atoms are involved in hydrogen bonding so that their environments differ (see supplementary material). To verify that the latter was taken into account in the model appropriately, we have compared a second multipole model for CL-20, where all the individual O atoms were freely refined. Although there is an indication of disorder (< 5%) in the NO₂ group of N9, we found that the physically most reliable multipole parameters can be obtained using the highly constrained multipole model. Furthermore, apart from the NO₂ group mentioned, only very subtle differences were found in a comparison of the electron density of the two models, leading us to the conclusion that the inclusion of the averaged intermolecular interaction is indeed appropriate. For FOX-7 an analogous procedure was followed and two multipole models were compared. In the ‘high-symmetry’ model the following constraints were used: O12,21 and 22 were constrained to O11, N21 to N11, N22 to N21 and H12,21,22 to H11. In the lower-symmetry model all the O atoms were refined independently, again supporting the adequate performance of the high-symmetry model, so that results are only reported for this model. The local atomic site symmetry chosen was m for N11/12, 2 for the C atoms and cylinder symmetry (6) for the H atoms, whereas all multipoles were refined for the O and the N21/22 atoms. In all the models mentioned l_{max} for H atoms was 2, including only one bond-directed quadrupole. Bond distances to H atoms were set to standard neutron distances. In both refinements the Hirshfeld test (Hirshfeld, 1976) is fulfilled, with the largest difference in the mean-square displacement amplitudes being $8 \times 10^{-4} \text{ \AA}^2$ for CL-20 and $5 \times 10^{-4} \text{ \AA}^2$ for FOX-7.

Single-point energy calculations using the program GAUSSIAN98 (Frisch *et al.*, 2002) and the experimental geometry were performed to obtain theoretical electron densities. Simulated structure factors not taking into account thermal motion were subsequently calculated by Fourier transform (Jayatilaka, 1994) with the program TONTO (Jayatilaka & Grimwood, 2003) for reciprocal lattice points of a cubic cell of 30 Å (centrosymmetric space group $P\bar{1}$) up to a resolution of $\sin \theta/\lambda = 1.15 \text{ \AA}^{-1}$. Molecules were placed at approximately $\frac{1}{4}, \frac{1}{4}, \frac{1}{4}$ of this unit cell and the contribution of the core electrons was included in structure-factor calculations. The same ‘high-symmetry’ multipole models as mentioned above were also applied to the theoretically simulated structure factors to allow a comparison of topological properties unbiased by the density description, yielding an R factor of 0.015 for CL-20 and 0.008 for FOX-7. The procedure allows a comparison of topological parameters free of the multipole-model bias.

3.2. Calculation of ADPs for H atoms for FOX-7

In order to avoid the influence of the thermal motion of the H atoms on the electron density of the heavier atoms (Madsen

Table 3

Comparison of bond-topological properties for CL-20 between theory [DFT, projected onto the multipole model, basis B3LYP/6-31++G(d,p), lower entries] and experimental results (upper entries).

ρ and $\nabla^2\rho$ denote the electron density and the Laplacian at the bond-critical point. ϵ is the bond ellipticity and d is the distance from the first atom defining the bond to the critical point. Units are in e and Å.

Bond	$\rho(\mathbf{r}_{\text{bcp}})$	$\nabla^2(\mathbf{r}_{\text{bcp}})$	d	ϵ
O1–N1	3.23 (2)	–9.2 (1)	0.6712	0.11
	3.13	–6.1	0.6430	0.13
O2–N1	3.36 (2)	–14.5 (1)	0.6654	0.10
	3.23	–8.5	0.6377	0.15
O3–N3	3.23 (2)	–9.2 (1)	0.6711	0.11
	3.13	–6.095	0.6430	0.13
O4–N3	3.30 (2)	–12.9 (1)	0.6685	0.10
	3.16	–7.2	0.6412	0.14
O5–N5	3.17 (2)	–7.8 (1)	0.6743	0.11
	3.07	–5.0	0.6464	0.13
O6–N5	3.33 (2)	–13.7 (1)	0.6667	0.10
	3.20	–7.8	0.6393	0.14
O7–N7	3.28 (2)	–10.4 (1)	0.6684	0.11
	3.19	–7.2	0.6400	0.13
O8–N7	3.31 (2)	–13.2 (1)	0.6678	0.10
	3.17	–7.4	0.6405	0.14
O9–N9	3.01 (2)	–1.0 (1)	0.6836	0.05
	2.87	3.4	0.6577	0.10
O10–N9	3.13 (2)	–5.7 (1)	0.6762	0.11
	2.96	–0.3	0.6515	0.12
O11–N11	3.01 (2)	–0.9 (1)	0.6840	0.05
	2.86	3.5	0.6581	0.10
O12–N11	3.15 (2)	–6.1 (1)	0.6751	0.11
	2.98	–0.6	0.6504	0.12
N1–N2	2.14 (2)	–2.9 (1)	0.6964	0.21
	2.13	–4.7	0.7064	0.21
N3–N4	2.29 (1)	–4.8 (1)	0.6804	0.20
	2.27	–6.7	0.6904	0.19
N5–N6	2.31 (3)	–6.1 (1)	0.6792	0.35
	2.27	–7.1	0.6907	0.25
N7–N8	2.24 (1)	–4.3 (1)	0.6849	0.22
	2.23	–6.2	0.6950	0.22
N9–N10	1.95 (1)	1.8 (1)	0.6994	0.15
	1.92	0.6	0.7086	0.17
N11–N12	1.98 (1)	1.6 (1)	0.6956	0.17
	1.95	0.4	0.7048	0.18
N2–C1	1.88 (1)	–14.0 (1)	0.8102	0.06
	1.88	–14.7	0.8062	0.04
N2–C3	1.85 (1)	–12.8 (1)	0.8083	0.07
	1.86	–13.8	0.8070	0.04
N4–C3	1.75 (1)	–10.4 (1)	0.8173	0.07
	1.76	–11.1	0.8131	0.10
N4–C5	1.80 (1)	–10.9 (1)	0.8086	0.08
	1.82	–12.1	0.8103	0.13
N6–C5	1.82 (1)	–12.0 (1)	0.8063	0.10
	1.82	–12.9	0.8012	0.14
N6–C7	1.77 (1)	–11.0 (1)	0.8133	0.09
	1.77	–11.4	0.8041	0.09
N8–C7	1.87 (1)	–13.8 (1)	0.8096	0.05
	1.88	–14.4	0.8054	0.05
N8–C9	1.86 (1)	–13.4 (1)	0.8094	0.05
	1.86	–14.0	0.8051	0.05
N10–C9	1.78 (1)	–11.2 (1)	0.8155	0.08
	1.79	–11.9	0.8114	0.10
N10–C11	1.77 (1)	–10.2 (1)	0.8095	0.10
	1.80	–11.7	0.8112	0.08
N12–C1	1.73 (1)	–9.0 (1)	0.8115	0.10
	1.76	–10.3	0.8122	0.07
N12–C11	1.82 (1)	–12.3 (1)	0.8138	0.08
	1.82	–12.9	0.8099	0.06
C1–C9	1.61 (1)	–11.2 (1)	0.7912	0.08
	1.60	–11.7	0.7914	0.11
C3–C7	1.61 (1)	–11.3 (1)	0.7907	0.08
	1.60	–11.8	0.7908	0.11

Table 3 (continued)

Bond	$\rho(\mathbf{r}_{\text{bcp}})$	$\nabla^2(\mathbf{r}_{\text{bcp}})$	d	ϵ
C5–C11	1.57 (1)	–10.7 (1)	0.7975	0.09
	1.57	–11.2	0.7975	0.12

et al., 2004), the anisotropic displacement parameters (ADPs) of the H atoms were calculated for FOX-7 with the TLS + ONIOM approach (Whitten & Spackman, 2006), which is based on quantum mechanical/molecular mechanics (QM/MM) methodology (Dapprich *et al.*, 1999). A cluster of molecules was generated consisting of 13 molecules (Dittrich, 2007), see Fig. 3. The basis set 6-31G(d,p) was used for a quantum-mechanical geometry optimization of the central molecule in the high layer with the program GAUSSIAN98 (Frisch *et al.*, 2002). All the surrounding molecules were chosen to be a low layer and were treated with molecular mechanics employing the UFF force field (Rappé *et al.*, 1992). Frequencies (normal modes) resulting from the geometry optimization were evaluated with a slightly modified version of the XDVIB1/2 programs of the XD suite (Koritsánszky *et al.*, 2003). To obtain only the internal frequencies of the central molecule from the calculation an almost infinite atomic weight was assigned to the low-layer atoms. After transforming the calculated frequencies to the Cartesian crystal system omitting the lowest six normal modes calculated internal contributions were subtracted from the C,N,O atom ADPs. A subsequent TLS fit was performed on the C, N, O molecular skeleton with the program THMA11 (Schomaker & Trueblood, 1998). The sum of the TLS rigid-body contribution and the calculated internal contributions of the H atoms then yielded ADPs for H atoms in the Cartesian crystal frame. Full details of the general procedure used can be found in Whitten & Spackman (2006).

4. Results and discussion

In the low-resolution structure of CL-20 reported recently (Bolotina *et al.*, 2004) disorder has not been detected.

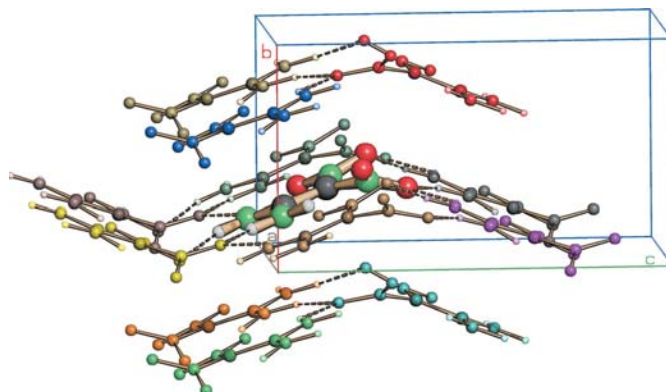


Figure 3 Molecular cluster for ADP calculation for FOX-7 consisting of 13 molecules visualized by SCHAKAL99 (Keller & Pierrard, 1999).

Table 4

Comparison of bond-topological properties for FOX-7 between theory [DFT, projected onto the multipole model, basis B3LYP/6-31++G(d,p), lower entries] and experimental results (upper entries).

ρ and $\nabla^2\rho$ denote the electron density and the Laplacian at the bond-critical point. ϵ is the bond ellipticity and d is the distance from the first atom defining the bond to the CP. Units are in e and Å.

Bond	$\rho(\mathbf{r}_{\text{bcp}})$	$\nabla^2\rho(\mathbf{r}_{\text{bcp}})$	d	ϵ
O11–N11	3.25 (2)	–5.5 (1)	0.6252	0.09
	3.13	–2.95	0.6153	0.08
O12–N11	3.21 (2)	–6.4 (1)	0.6287	0.10
	3.13	–3.42	0.6154	0.09
O21–N12	3.17 (2)	–4.0 (1)	0.6294	0.09
	3.05	–1.66	0.6195	0.08
O22–N12	3.16 (2)	–5.5 (1)	0.6313	0.10
	3.08	–2.61	0.6182	0.09
N11–C1	1.97 (1)	–17.0 (1)	0.8436	0.25
	1.96	–13.91	0.8230	0.26
N12–C1	2.01 (1)	–19.8 (1)	0.8438	0.32
	2.04	–16.30	0.8187	0.35
N21–C2	2.53 (1)	–25.8 (1)	0.7481	0.26
	2.40	–23.61	0.7489	0.25
N22–C2	2.56 (1)	–27.2 (1)	0.7487	0.24
	2.43	–24.85	0.7488	0.25
C1–C2	1.95 (1)	–14.2 (1)	0.7129	0.22
	1.85	–11.70	0.7054	0.33

However, we find that for one of the NO₂ groups (N11, O11, O12) static disorder in two discrete sites of 5 and 95% occurs and there is an additional peak close to O8. Including this disorder in the structural model did not improve the figures-of-merit and we therefore chose to average the electron density of the affected group with the other chemically equivalent NO₂ groups.

Owing to the disorder we restrain ourselves to a topological analysis of the chemically constrained electron-density model as described above for CL-20, whereas for FOX-7 a thorough analysis follows.

In order to compare theoretical and experimental electron densities the isolated molecular density was evaluated *via* simulated structure factors projected onto the multipole model. As described above, the agreement between experiment and theory is better than for similar comparisons performed earlier, for example in Dittrich *et al.* (2000), and chemical trends can be discussed. The agreement between ϵ and d , the bond ellipticity and the distance to the bond-critical point, especially improves and differences in topological properties can therefore be understood and interpreted free of model bias. In general, the agreement between experiment and theory is very good for the electron density $\rho(\mathbf{r}_{\text{bcp}})$ and the bond ellipticity ϵ , and good for the Laplacian ($\nabla^2\rho(\mathbf{r}_{\text{bcp}})$). While the electron density of the C–C, N–N and N–C bonds is almost identical for experiment and theory, the electron density of N–O bonds in the crystal exceeds the theoretical isolated molecular result in a systematic way.

For FOX-7 a topological analysis of the electron density has also been performed (Table 4). One can again observe that the experimental electron density is systematically higher for the

N–O bonds that are involved in hydrogen bonding than the projected theoretical result. This indicates that in the crystal the molecule has an increased stability compared with the gas phase. These results in principle support theoretical findings (Rice & Hare, 2002), as they indicate charge build-up of covalent bonds in the crystal. Whereas the agreement between theory and experiment is good in general, an interesting difference is found for the ellipticity ϵ of the C1–C2 bond, which might signal a different character of the bond for the isolated molecule and the molecule in the crystal. The interaction density, which is defined as ‘the difference between the electron density of the crystal and that arising from a super-

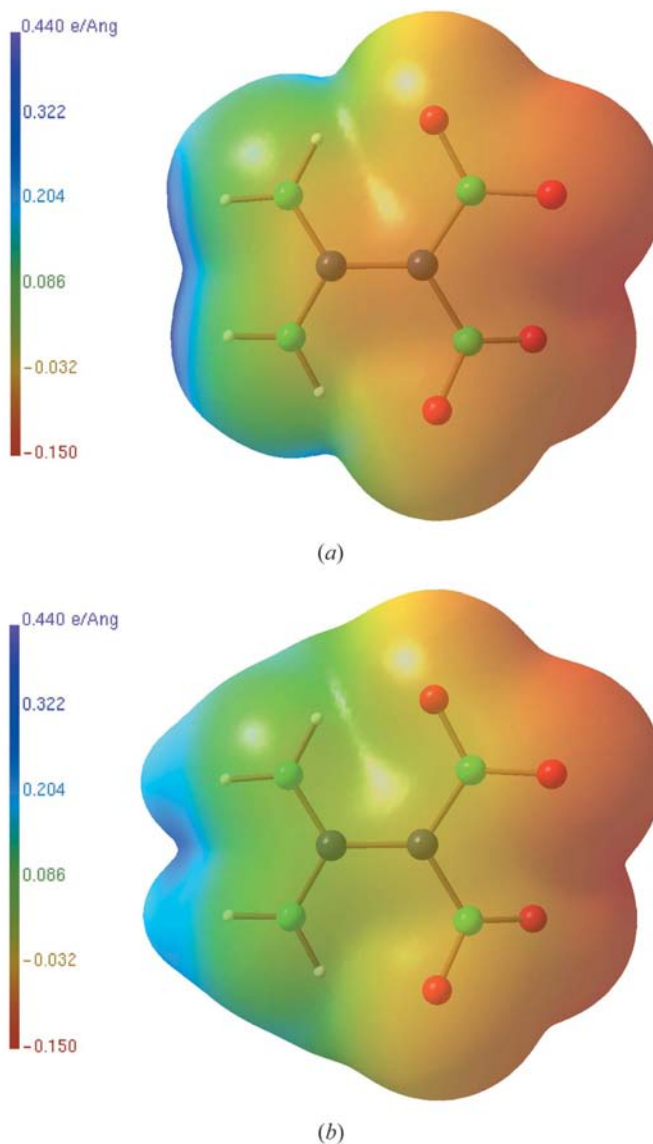


Figure 4
Electrostatic potential of FOX-7 mapped on an $0.0067 \text{ e } \text{Å}^{-3}$ iso-surface of electron density (corresponding to the commonly used theoretical value of $0.001 \text{ e bohr}^{-1}$) using the same scale (maximum negative value $-0.15 \text{ e } \text{Å}^{-1}$, maximum positive value $0.44 \text{ e } \text{Å}^{-1}$, both according to color code). **a** was calculated from the experimentally determined multipole parameters; **b** was derived from the multipole-projected isolated molecular calculation.

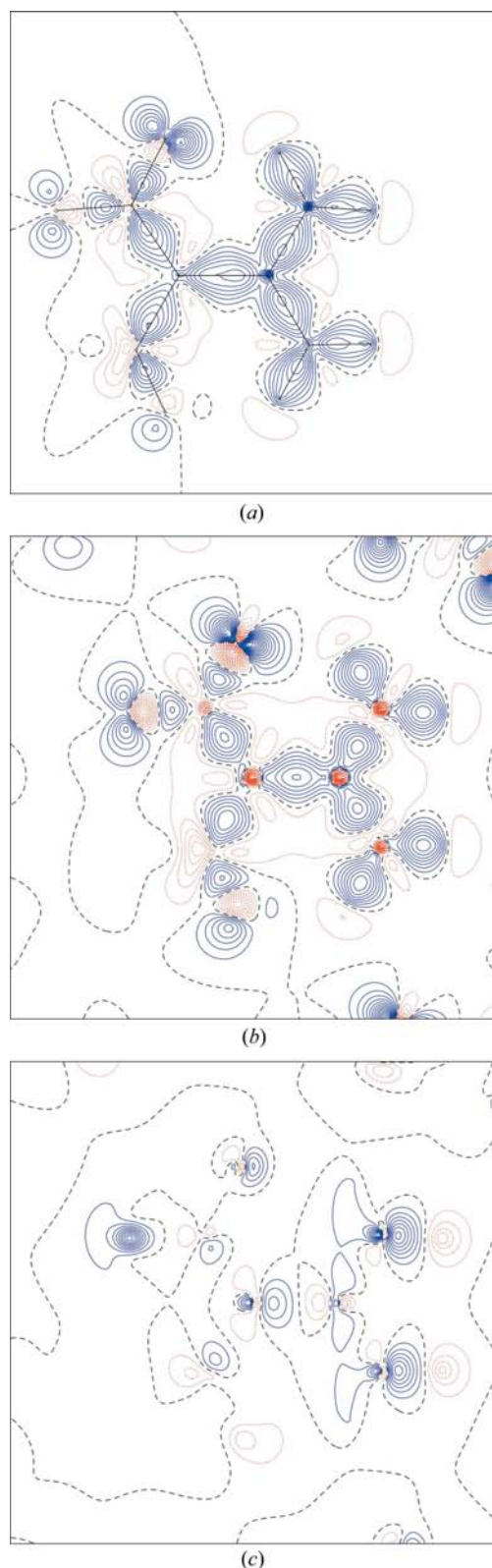


Figure 5
 (a) Experimental and (b) theoretical deformation density plot for FOX-7, and (c) interaction density plot using the same basis in the C1–C2–N22 plane, as calculated with *CRYSTALS98* using the *molsplit* option and the basis set HF/6-31G(d,p). For the deformation density plots contours of $0.1 \text{ e } \text{Å}^{-3}$ were chosen, whereas for the interaction density each contour represents $0.025 \text{ e } \text{Å}^{-3}$.

position of isolated molecules, positioned as in the crystal' (Spackman *et al.*, 1999), is investigated below.

Molecular electrostatic potentials have been calculated from both the theoretical and experimental multipole model electron densities according to the method by Su & Coppens (1992), were visualized with the program *MOLISO* (Hübschle & Luger, 2006) and are displayed in Fig. 4. Murray *et al.* (1995) suggest that a key factor in determining the impact sensitivities of these compounds may be the extent to which the stabilizing effect of charge delocalization has been counteracted. This hypothesis was based on a number of isolated molecule calculations. We observe quite pronounced differences in the ESPs between theory and experiment. Electro-positive maxima for FOX-7 occur at the site of the hydrogen-bonded hydrogen atoms H11 and H21 that are pointing directly at the accepting oxygen atoms O11 and O22 with a $D \cdots H-A$ angle close to 180° (supplementary material). As hydrogen bonding is the main difference between the molecule in the crystal and the isolated molecules, these fine differences in the electron density are relevant to the discussion, and differences between experimental electron density and isolated molecular theoretical ESPs are probably greater than the effects the hypothesis (Murray *et al.*, 1995) was based upon.

Further indications of the difference between isolated molecular and crystal electron densities can be provided by theory. Following Spackman and co-workers we have calculated the interaction density of FOX-7 using the *MOLSPLIT* option in the *CRYSTAL98* software (Saunders *et al.*, 1998) using the basis set HF/6-31G(d,p). The C1–C2–N22 plane was chosen to display these differences, as depicted in Fig. 5. First, the C1–C2 bond shows additional electron density in the crystal, agreeing with the difference in the value of ϵ mentioned above. In the interaction density plot the most pronounced differences of up to $0.18 \text{ e } \text{Å}^{-3}$ occur in the covalent N–H bonds of the NH_2 groups. Whereas the electron density distribution of the H atoms not involved in intermolecular hydrogen bonding does not change markedly, the covalent N–H bonds of the H atoms involved in such interactions get stronger. Core polarization of the O atom in the plane of the molecule can also be seen on the left of the map. All these differences are along the main plane of the molecule, so an increase of the dipole moment is expected.

Table 5 lists the experimental and theoretical results of the dipole moments that were obtained directly from theory, from the multipole-projected theoretical result and from experiment. Surprisingly, the theoretical result derived *via* calculated structure factors simulating an experiment is higher than directly from theory. It seems that there is a false 'enhancement' of the dipole moment just from the density model used. Apart from that difference due to the modelling, the experimental dipole moment and the theoretical results agree quite well, which also holds for the individual components. Taking into account three standard deviations of the experimental dipole moment it remains unclear whether there is an enhancement in the crystal or not.

Table 5
Dipole moments for FOX-7.

Molecule	Method	Dipole moment (D)			Total
		x	y	z	
FOX-7	Experimental multipole refinement	-4.2 (2)	-3.3 (2)	-9.5 (4)	10.8 (4)
	Theoretical (multipole projected) B3LYP/6-31++G(d,p)	-4.6 (1)	-3.8 (1)	-10.7 (1)	12.3 (1)
	Direct from theory B3LYP/6-31++G(d,p)	-3.9	-3.1	-8.3	9.7

5. Conclusion

The experimental charge densities of CL-20 and FOX-7, two energetic materials, were determined from high-resolution single-crystal diffraction data and their electron-density derived properties were determined. Calculated hydrogen ADPs enabled a full analysis of the FOX-7 data, whereas small but noticeable disorder limits the reliable information that can be obtained for CL-20. Using a projection of the theoretical density onto the multipole model, differences in the topological analysis of isolated molecular and crystal electron densities were discussed. Subtle differences in theoretical ESPs of different molecules that were used to explain and predict impact sensitivities in the literature are probably smaller than differences between experiment for bulk molecules and theory for an isolated molecule. It is therefore difficult to verify or refute such hypotheses. However, we want to say that based on such differences some scepticism that the isolated molecular ESP can provide predictions of impact sensitivity, which is a bulk property, might be appropriate. Dipole moments derived from experiment agree well with theoretical findings and a small increase in the molecular dipole moment – but within the error range of the determination – was found.

With the considerable number of explosives studied by high-resolution X-ray diffraction it is recommended that future theoretical studies use the accurate geometries determined this way and include investigations of properties of molecules in the crystal environment rather than being limited to isolated molecular properties, as the crystal field probably plays an important role for impact sensitivities and alters other relevant properties.

This work was supported by the Australian Synchrotron Research Program (ASRP), which is funded by the Commonwealth of Australia under the Major National Research Facilities Program. BD thanks the ASRP for a postdoctoral fellowship.

References

- Bader, R. F. W. (1990). *Atoms in Molecules: A Quantum Theory*, 1st ed. Oxford: Clarendon Press.
- Bemm, U. & Östmark, H. (1998). *Acta Cryst.* **C54**, 1997–1999.
- Bolotina, N. B., Hardie, M. J., Speer Jr, R. L. & Pinkerton, A. A. (2004). *J. Appl. Cryst.* **37**, 808–814.
- Burnett, M. N. & Johnson, C. K. (1996). *ORTEP* III, Report ORNL-6895. Oak Ridge National Laboratory, Tennessee, USA.

- Chen, Y.-S., Stash, A. I. & Pinkerton, A. A. (2007). *Acta Cryst.* **B63**, 309–318.
- Coppens, P. (1997). *X-ray Charge Densities and Chemical Bonding*, No. 4 in IUCr Texts on Crystallography, 1st ed. Oxford University Press.
- Dapprich, S., Komáromi, I., Byun, K. S., Morokuma, K. & Frisch, M. J. (1999). *J. Mol. Struct. Theochem.* **461**, 1–21.
- Dittrich, B. (2007). *TLS+O*. Technical Report. University of Western Australia, Crawley, WA.
- Dittrich, B., Flaig, R., Koritsánszky, T., Krane, H.-G., Morgenroth, W. & Luger, P. (2000). *Chem. Eur. J.* **6**, 2582–2589.
- Frisch, M. J. *et al.* (2002). *GAUSSIAN98*, Revision A.11.3. Technical Report. Gaussian, Inc., Pittsburgh PA.
- Gilardi, R. (1999). Private communication (deposition number 127539). Cambridge Structural Database, Cambridge, England.
- Hansen, N. K. & Coppens, P. (1978). *Acta Cryst.* **A34**, 909–921.
- Hirshfeld, F. L. (1976). *Acta Cryst.* **A32**, 239–244.
- Hübschle, C. B. & Luger, P. (2006). *J. Appl. Cryst.* **39**, 901–904.
- Jayatilaka, D. (1994). *Chem. Phys. Lett.* **230**, 228–230.
- Jayatilaka, D. & Grimwood, D. J. (2003). *Computational Science – ICCS 2003*, **2660**, 142–151.
- Johnas, S. K. J., Morgenroth, W. & Weckert, E. (2006). *HasyLab Jahresber.*
- Kabsch, W. (1993). *J. Appl. Cryst.* **26**, 795–800.
- Keller, E. & Pierrard, J.-S. (1999). *SCHAKAL99*. Technical Report. University of Freiburg, Germany.
- Kempa, P. B. & Herrmann, M. (2005). *Part. Part. Syst. Char.* **22**, 418–422.
- Koritsánszky, T., Richter, T., Macchi, P., Volkov, A., Gatti, C., Howard, S., Mallinson, P. R., Farrugia, L., Su, Z. W. & Hansen, N. K. (2003). *XD*. Technical Report. Freie Universität Berlin, Germany.
- Madsen, A. Ø., Sørensen, H. O., Flensburg, C., Stewart, R. F. & Larsen, S. (2004). *Acta Cryst.* **A60**, 550–561.
- Murray, J. S., Lane, P. & Politzer, P. (1995). *Mol. Phys.* **85**, 1–8.
- Nielsen, A. T., Chafin, A. P., Christian, S. L., Moore, D. W., Nadler, M. P., Nissan, R. A. & Vanderah, D. J. (1998). *Tetrahedron*, **54**, 11793–11812.
- Rappé, A. K., Casewit, C. J., Colwell, K. S., Goddard, W. A., Skid, W. M. & Bernstein, E. R. (1992). *J. Am. Chem. Soc.* **114**, 10024–10039.
- Rice, B. M. & Hare, J. J. (2002). *J. Phys. Chem. A*, **106**, 1770–1783.
- Russell, T. P., Miller, P. J., Piermarini, C. J. & Block, S. (1993). *J. Phys. Chem.* **97**, 1993–1997.
- Saunders, V. R., Dovesi, R., Roetti, C., Causà, M., Harrison, N. M., Orlando, R. & Zicovich-Wilson, C. (1998). *CRYSTAL98 User's Manual*. Technical Report. Università di Torino, Torino, Italy.
- Schomaker, V. & Trueblood, K. N. (1998). *Acta Cryst.* **B54**, 507–514.
- Sorescu, D. C., Boatz, J. A. & Thompson, D. L. (2001). *J. Phys. Chem. A*, **105**, 5010–5021.
- Sorescu, D. C., Rice, B. M. & Thompson, D. L. (1998). *J. Phys. Chem. B*, **102**, 948–952.
- Spackman, M. A., Byrom, P. G., Alfredsson, M. & Hermansson, K. (1999). *Acta Cryst.* **A55**, 30–47.
- Stewart, R. F. (1976). *Acta Cryst.* **A32**, 565–574.
- Su, Z. & Coppens, P. (1992). *Acta Cryst.* **A48**, 188–197.
- Whitten, A. E. & Spackman, M. A. (2006). *Acta Cryst.* **B62**, 875–888.
- Zaleski, J., Wu, G. & Coppens, P. (1998). *J. Appl. Cryst.* **31**, 302–304.
- Zhurova, E. A. & Pinkerton, A. A. (2001). *Acta Cryst.* **B57**, 359–365.
- Zhurova, E. A., Stash, A. I., Mikhail, V. V. Z., Barthashevich, E. V., Potemkin, V. A. & Pinkerton, A. A. (2006). *J. Am. Chem. Soc.* **128**, 14728–14734.
- Zhurova, E. A., Tsirelson, V. G., Stash, A. I., Yakovlev, M. V. & Pinkerton, A. A. (2004). *J. Phys. Chem. B*, **108**, 20173–20179.